Applied Catalysis B: Environmental 129 (2013) 225–235

Contents lists available at SciVerse ScienceDirect

Applied Catalysis B: Environmental

journal homepage: www.elsevier.com/locate/apcatb

Promoted activity of sulphated Ce/Zr mixed oxides for chlorinated VOC oxidative abatement

B. de Rivas, C. Sampedro, M. García-Real, R. López-Fonseca, J.I. Gutiérrez-Ortiz*

Department of Chemical Engineering, Faculty of Science and Technology, Universidad del País Vasco UPV/EHU, PO Box 644, E-48080, Bilbao, Spain

ARTICLE INFO

Article history:
Received 6 June 2012
Received in revised form
13 September 2012
Accepted 15 September 2012
Available online 26 September 2012

Keywords:
Chlorinated VOCs
Catalytic oxidation
1,2-Dichloroethane
Ce/Zr mixed oxides
Sulphation
Acidity

ABSTRACT

The catalytic oxidative decomposition of 1,2-dichoroethane was examined over a series of Ce/Zr mixed oxides (CeO_2, $Ce_{0.8}Zr_{0.2}O_2$, $Ce_{0.5}Zr_{0.5}O_2$, $Ce_{0.15}Zr_{0.85}O_2$ and ZrO_2) treated with a 1 M aqueous solution of H_2SO_4 or HNO_3. After calcination at 550 °C, the doped samples were characterised by dynamic thermogravimetry, X-ray diffraction, N_2-physisorption, Raman spectroscopy, X-ray photoelectron spectroscopy, temperature-programmed desorption of ammonia, adsorption of pyridine followed by Raman spectroscopy and temperature-programmed reduction with hydrogen. A noticeable promotion of activity was found for all sulphated oxides, which was associated with an increase of the total acidity and more particularly with a higher concentration of sites with a moderate/strong acid strength. Also the generation of new Brönsted acid sites was found. Interestingly, sulphation did not lead to a significant loss of surface area (except for sulphated ceria) and redox properties linked to the Ce^{4+}/Ce^{3+} cycle were not apparently affected. Sulphated $Ce_{0.5}Zr_{0.5}O_2$ and $Ce_{0.15}Zr_{0.85}O_2$ samples showed the highest catalytic activity. Hence, the temperatures for DCE removal (in terms of T_{50} and T_{90}) were considerably lowered by 80 °C (T_{50}) and 120 °C (T_{90}). This behaviour evidenced that sulphation was an effective tool to improve the performance of Ce/Zr mixed oxides for chlorinated VOC abatement. In contrast, the activity of the samples modified with nitric acid hardly showed any variation.

1. Introduction

Increasing concern over detrimental environmental and health effects resulting from emission of volatile organic compounds (VOCs) has led to stricter emissions regulation standards [1], and has fuelled efforts to identify efficient and economical methods for VOC abatement [2]. Notably, chlorine-containing organic compounds require a special attention due to their distinct toxicity, high stability and persistence in the environment. Even so, these compounds are widely used in a variety of industries for a range of purposes (manufacture of herbicides and plastics, manufacture and use of solvents in the automotive, aerospace, garment and electronic industries) since they are compatible with most substrate materials and are non-flammable. Several different technologies have been developed for chlorinated VOC abatement, but one of the most versatile is catalytic oxidation. This strategy offers the advantage that dilute VOCs (<0.1%) can be removed from effluents to very low levels. More importantly, in contrast to thermal incineration, the lower temperatures used (300–550 °C) result in a more economical process, and the potential for the production of toxic by-products such as dioxins and NO_x is significantly reduced.

The design of alternative efficient catalysts to costly noble metals is probably the most important challenge for researchers when dealing with the oxidation of chlorinated VOCs. The requirements are very demanding since, apart from exhibiting a high intrinsic activity as large gas volumes have to be typically treated (>10,000 h^{-1}), the catalyst must favour the conversion to HCl and CO_2 as the preferred decomposition products with a limited yield of chlorinated by-products (in some cases even more toxic than the starting chlorocarbon). Note that, in some cases, a marked oxidation ability promotes the yield of CO_2 but also the formation of Cl_2 as a result of the activation of the Deacon reaction. In addition, the ideal catalyst must be relatively cheap and show a notable stability. Deactivation is usually related to chlorine-poisoning and/or coke formation (particularly when abating chlorinated hydrocarbons with high H/Cl ratios) [3].

On the basis of our previous studies Ce/Zr mixed oxides appear as attractive candidates for this environmental application. These bulk catalysts present an adequate combination of acid and redox properties that results in a notable performance of the oxidation of 1,2-dichloroethane and trichloroethylene [4,5]. Interestingly, they are highly resistant to thermal aging and induced chlorine-poisoning [6,7]. In order to improve their behaviour the attention

* Corresponding author. Tel.: +34 94 6012683; fax: +34 94 6015963.
E-mail address: joseignacio.gutierrez@ehu.es (J.I. Gutiérrez-Ortiz).

0926-3373/$ – see front matter © 2012 Elsevier B.V. All rights reserved.
http://dx.doi.org/10.1016/j.apcatb.2012.09.026

was focused on examining effective strategies to promote these key catalytic properties. Hence, the application of specific high-temperature redox treatments led to a substantially improved redox behaviour through the formation of pyrochlores [8]. As for the acid properties, the use of zeolites (H-ZSM5 or USY) as acidic supports for CeO_2 was also successfully explored [9,10]. In this paper an alternative approach to enhance the acid properties of the Ce/Zr mixed oxides was examined. Particularly, the influence of surface sulphation was investigated. Some previous studies on the efficient use of sulphated catalysts for halogenated VOC destruction are available in the technical literature. For example, Feaver and Rossin evaluated the catalytic decomposition of CHF_3 over sulphated zirconia [11] and Park et al. investigated the oxidative degradation of trichloroethylene over sulphated zirconia supported palladium catalysts [12]. In both cases a promoted catalytic behaviour caused by sulphation was observed. More recently, Gaigneaux et al. have reported the beneficial effect of sulphation of several vanadia-based materials for the total oxidation of chlorobenzene [13,14].

Therefore, the scope of this study was to evaluate the catalytic behaviour of a series of sulphated Ce/Zr mixed oxides in the oxidative decomposition of chlorinated VOCs. Sulphation was conducted by impregnation with an aqueous solution of H_2SO_4. For comparative purposes, the use of HNO_3 as an alternative strong acid was also explored. Note that to the best of our knowledge no previous references are available regarding the effect of acidification of this type of mixed oxides for this environmental application. 1,2-Dichloroethane ($C_2H_4Cl_2$, DCE), also known as ethylene dichloride, was selected a as model chlorinated VOC since it is probably one of the most important chlorinated VOC emitted in gaseous industrial waste streams since it is used as an intermediate for the production of polyvinyl chloride, the most produced plastic in the world after polyethylene [15]. Less important uses are as a solvent in textile cleaning and metal degreasing and paint remover, a starting material for paint, varnish, and finish removers, a cleaner for upholstery and carpets, a fumigant, a lead scavenger in antiknock gasoline, and as a dispersant for plastics and elastomers such as synthetic rubber [16].

2. Experimental

2.1. Catalysts preparation

Ceria–zirconia mixed oxides with varying Ce/Zr ratio, including pure ceria, were supplied by Rhodia, while the zirconium oxide was provided by Norton. Hereafter, the samples will be referred to as CZXX/YY where XX and YY indicate the molar percentage of CeO_2 and ZrO_2, respectively. The catalysts (3 g) were treated with an aqueous solution (500 cm^3) of H_2SO_4 or HNO_3 1 M at 70 °C for 1 h under vigorous stirring. Then the samples were filtered, dried overnight at 110 °C and calcined at 550 °C in air for 4 h in static air. Finally, the oxide powders were pelleted, crushing and sieving to achieve pellets with diameter from 0.3 to 0.5 mm. The labelling code was modified by inserting a new character, namely 'S' for the oxides treated with sulphuric acid, and 'N' for the samples treated with nitric acid. Prior to catalytic activity and selectivity experiments all the doped samples were characterised using several analytical techniques.

2.2. Characterisation techniques

Dynamic thermogravimetric analysis (TGA) was performed in order to evaluate the sulphur and nitrogen content of the doped samples and the thermal stability of grafted species. These experiments were carried out using a Setaram Setsys Evolution apparatus under atmospheric pressure. The mass loss and the sample temperature were continuously recorded in the 25–1000 °C range by a computerised data acquisition system. The carrier stream was helium flowing downwards onto the cylindrical sample holder. The exit gaseous stream was analysed by mass spectrometry (MS, Pfeiffer Prisma). The data were recorded and processed using the Quadstar 32-Bit programme.

Textural properties were evaluated from the nitrogen adsorption–desorption isotherms, determined at −196 °C with a Micromeritics ASAP 2020 apparatus. The specific areas of the samples were determined according to the standard BET procedure using nitrogen adsorption taken in the relative equilibrium pressure interval of 0.03–0.3. Mean pore size was calculated from the BJH method. The samples were previously degassed overnight at 300 °C under high vacuum. X-ray diffraction (XRD) studies were carried out on a X'PERT-MPD X-ray diffractometer with Cu Kα radiation (λ = 1.5406 Å) and Ni filter. The X-ray tube was operated at 30 kV and 20 mA. Samples were scanned from $5° < 2\theta < 80°$ and the X-ray diffraction line positions were determined with a step size of 0.02° and counting time of 2.5 s per step.

Raman spectra, acquired using a Leica 50×N Plan (0.75 aperture) lens, were recorded with a Renishaw InVia Raman spectrometer coupled to a Leica DMLM microscope. The spectrometer was equipped with a 514 nm laser (ion-argon laser, Modu-Laser) with a nominal power at the source of 50 mW, with maximum power at the sample of 20 mW. 10 s were employed for each spectrum, and 20 scans were accumulated with 10% of the maximum power in the spectral window from 150 to 3200 cm^{-1}. This technique was used, on one hand, as a tool for evidencing the presence of S- or N-containing species on the doped oxides. On the other hand, after adsorption of pyridine vapours at 100 °C up to saturation, Raman spectroscopy was also helpful in identifying the nature of acid sites present on the catalysts after impregnation with the strong acids.

Sulphated samples were additionally were characterised by X-ray photoelectron spectroscopy (XPS). XPS measurements were performed with a Phoibos 150 1D-DLD analysis system from Specs. Photoelectrons were excited with the AlKα line. The hemispheric photoelectron analyser worked with a pass energy of 20 eV. In order to compare all spectra recorded, the C1s core level attributable to adventitious carbon present in the samples was selected as a reference, whose binding energy was fixed to 284.6 eV.

Temperature-programmed desorption (TPD) of ammonia was performed on a Micromeritics Autochem 2920 instrument equipped with a quartz U-tube coupled to a thermal conductivity detector. Prior to adsorption experiments, the samples (30 mg) were first pre-treated in a 5%O_2/He stream at 550 °C. Then, they were cooled down at 100 °C in a He flow (20 cm^3 min^{-1}). Later, the NH_3 adsorption step was performed by admitting a flow of 10%NH_3/He at 100 °C up to saturation. Subsequently, the samples were exposed to a flow of helium (50 cm^3 min^{-1}) for 1 h at 100 °C in order to remove reversibly and physically bound ammonia from the surface. Finally, desorption was carried out from 100 to 550 °C at a heating rate of 10 °C min^{-1} in a He stream (50 cm^3 min^{-1}). This temperature was maintained for 1 h until the adsorbate was completely desorbed. The amount of gases desorbed was determined by time integration of the TCD curves. The composition of the exit stream was followed by a mass spectrometer (Pfeiffer Prisma).

Redox behaviour was examined by temperature-programmed reduction experiments (TPR). These experiments were conducted on a Micromeritics Autochem 2920 instrument as well. Firstly, all the samples were pre-treated in an oxygen stream (5% O_2/He) at 550 °C for 1 h, and then cooled down to room temperature. The reducing gas used in all experiments was 5% H_2 in Ar, with a flow rate of 50 cm^3 min^{-1}. The temperature range explored was from room temperature to 950 °C with a heating rate of 10 °C min^{-1}. This temperature was maintained for 0.5 h so as to complete the

reduction process. The water produced by reduction was trapped into a cold trap. The consumption of H_2 was quantitatively measured by time integration of TPR profiles. The TPR flow exit was also analysed by a mass spectrometer.

2.3. Catalyst activity determination

Catalytic tests were performed in a bench-scale fixed bed reactor (Microactivity modular laboratory system provided by PID Eng&Tech S.L.) operated at atmospheric pressure and fully monitored by computer. The reactor was made of quartz with an internal diameter of 10 mm and a height of 300 mm, in which the temperature is controlled with a thermocouple place in the catalyst bed. Typically 0.85 g of catalyst in powdered form (0.3–0.5 mm) was loaded. The reaction feed consisted of 1000 ppm of DCE in dry air with a total gas flow of 500 $cm^3 min^{-1}$. The amount and granulometric fraction of catalyst and the total gaseous stream were chosen in order to be in true kinetic regime, namely be out of the internal and external diffusion limits, and to reach a gas hourly space velocity of 30,000 h^{-1}, which corresponds to the conditions usually met in the exhaust gases from industrial units. Catalytic activity was measured over the range 150–550 °C and conversion data were calculated by the difference between inlet and outlet concentrations. Conversion measurements and product profiles were taken at steady state, typically after 30 min on stream. Either product selectivity was calculated based on either chlorine or carbon atoms present in that product divided by the total chlorine or carbon atoms present in the product stream (expressed as %). The feed and effluent streams were analysed using an on-line 7980A Agilent Technologies gas chromatograph equipped with a thermal conductivity (CO and CO_2) and an electron capture detector (chlorinated hydrocarbons). Analysis of HCl and Cl_2 was carried out by means of ion selective electrode and titration, respectively. Further details on analytical procedures are described elsewhere [17].

3. Results and discussion

3.1. Characterisation of the catalysts

To clarify the connection between changes in catalytic activity and those of surface structure/composition both fresh and doped samples, before they were subjected to catalytic activity experiments, were characterised by a number of analytical techniques. Since, as will be shown later, sulphation resulted in a more marked influence on catalytic performance, more attention was paid to these samples. Anyway, some results on characterisation of the nitrated samples were also provided.

Thermogravimetric analysis coupled to mass spectrometry was preliminary conducted in order to determine the amount of sulphur- or nitrogen-containing species present on the doped mixed oxides after calcination at 550 °C for 4 h. Fig. 1 includes the total weight loss curves resulting from heating from 50 to 1000 °C with flowing helium. The thermal protocol used is depicted in the graph, and included four isothermal steps at 50, 110, 550 and 1000 °C. The temperature was ramped at 10 °C min^{-1}. As an example, Fig. 1 also shows the analysis of the evolved gases by online MS during the TGA run over CZ50/50S and CZ50/50N samples. The mass signals corresponding to H_2O (m/z = 18), NO (m/z = 30), O_2 (m/z = 32), N_2O (m/z = 44), NO_2 (m/z = 46), SO_2 (m/z = 48 and m/z = 64) and H_2SO_4 (m/z = 98) were monitored.

For all the sulphur-doped samples a similar pattern with three major weight losses was observed. Hence, the first two weight losses at relatively low temperatures (<550 °C) were essentially assigned to desorption of water with a small contribution of CO_2 desorption (MS profiles not shown). No signals associated with the presence of sulphur-containing species were noticed in this temperature range, this revealing a relatively high stability of deposited compounds on the oxide catalysts. When the temperature was further increased a third, remarkable weight loss was recorded. As revealed by the prominent peaks detected at m/z = 48 and m/z = 64,

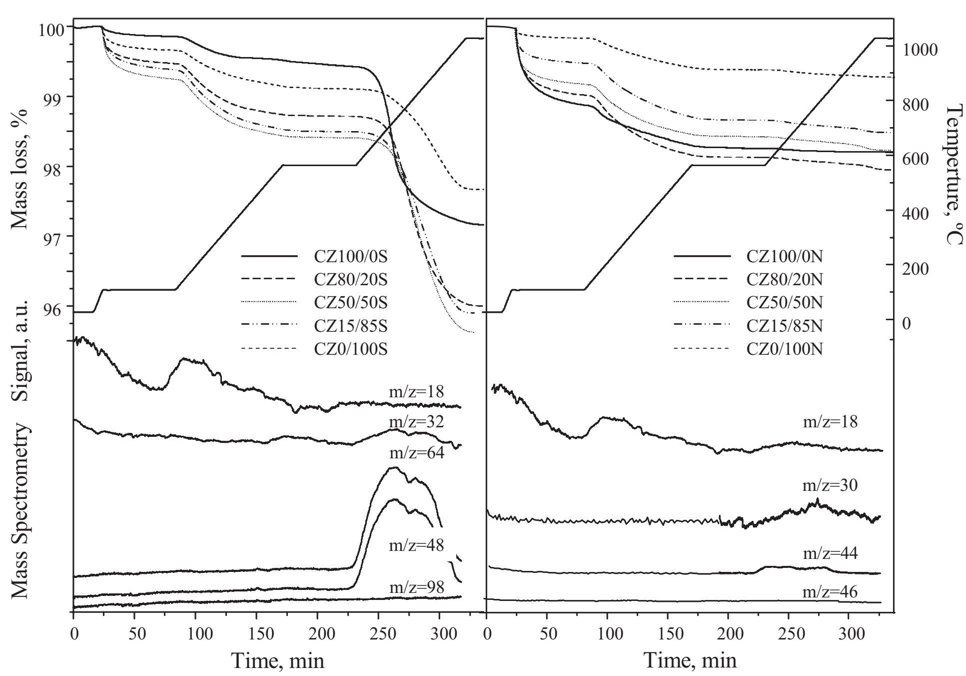

Fig. 1. Weight loss curves plotted as percent initial weight as a function of time and temperature for CZS and CZN samples. MS profile corresponding to TGA runs for CZ50/50S and CZ50/50N samples.

Table 1
Composition, textural and structural properties of CZ, CZS and CZN samples.

Catalyst	S content (TGA–MS/XPS), %	N content (TGA–MS), %	S_{BET}, $m^2\ g^{-1}$	V_p, $cm^3\ g^{-1}$	Average pore size, Å	Structure	Crystal size, nm
CZ100/0	–	–	99	0.21	60	cubic	9.9
CZ100/0S	1.0/1.7	–	35	0.14	143	cubic	21.1
CZ100/0N	–	0.03	96	0.19	61	cubic	16.5
CZ80/20	–	–	102	0.18	48	cubic	6.9
CZ80/20S	1.2/1.5	–	79	0.13	55	cubic	8.5
CZ80/20N	–	0.09	97	0.15	49	cubic	7.2
CZ50/50	–	–	99	0.21	64	tetragonal	7.0
CZ50/50S	1.3/2.0	–	98	0.18	63	tetragonal	7.0
CZ50/50N	–	0.10	87	0.19	71	tetragonal	8.0
CZ15/85	–	–	86	0.28	102	tetragonal	6.4
CZ15/85S	1.2/1.3	–	90	0.25	97	tetragonal	6.2
CZ15/85N	–	0.09	85	0.24	99	tetragonal	5.5
CZ0/100	–	–	51	0.25	157	monoclinic	14.5
CZ0/100S	0.6/0.7	–	47	0.19	157	monoclinic	17.1
CZ0/100N	–	0.06	50	0.20	141	monoclinic	12.0

this loss was clearly related to the release of gaseous SO_2 as a result of the thermal decomposition of surface sulphates under inert conditions probably via SO_3 formation (not observed by MS due to its high instability). It must be pointed out that the release of O_2 also took place in parallel to the release of SO_2. The flat signal at m/z = 98 (H_2SO_4) indicated the complete deprotonation of sulphuric acid on ceria–zirconia surfaces leading to adsorbed sulphate anions and surface hydroxyl groups [18,19].

The amount of sulphate groups present on the oxides was then determined from the overall mass loss due to the release of SO_2 between 550–1000 °C (end of mass loss due to sulphate groups). As shown in Table 1, it was found that the pure ceria (CZ100/0S) was sulphated to a larger extent when compared with pure zirconia (CZ0/100S). However, the Ce/Zr mixed oxides presented a slightly higher sulphur content, in the 1.2–1.3 wt.% range. As regards the nitrated samples, the TGA profiles displayed a substantial weight loss between 110 and 550 °C attributed to water desorption. Beyond this temperature a slight decrease could be noticed which was assigned to the decomposition of grafted species to NO (m/z = 30) and/or N_2O (m/z = 44). The nitrogen content of the samples (Table 1) was estimated from this loss and varied from 0.05 to 0.1 wt.%. The comparison of the compositions of CZS and CZN samples revealed that sulphation was more effective than nitration. In other words, the thermal stability of sulphated samples after calcination at 550 °C was markedly higher.

The CeO_2 sample (CZ100/0) showed well-defined diffraction peaks corresponding to a cubic structure. However, it should be pointed out that the most intense lines were shifted to significantly higher diffraction angles with increasing ZrO_2 content. This observation was attributed to shrinkage of lattice due to the replacement of Ce^{4+} with a smaller Zr^{4+} cation radius. It was noticed that the mixed oxide systems exhibited a solid solution structure in which the cation sublattice had a cubic structure for CZ80/20 oxide and a tetragonal structure for CZ50/50 and CZ15/85 samples. The presence of monoclinic phase was only observed in the pure ZrO_2 catalyst (CZ0/100). The assessment of formation of a solid solution during the synthesis process could be deduced by the analysis of XRD patterns. The diffractograms (not shown) corresponding to CZ80/20 and CZ50/50 oxides did not display peaks assigned to zirconia as segregated phases [4]. Therefore, it could be deduced that these mixed oxides were solid solutions. However, as for CZ15/85 sample, the appearance of two strongest lines of zirconia could be observed in the XRD pattern. This evidenced that this sample was not a homogeneous solution. According to Vegard's rule, due to the smaller Zr^{4+} ionic radius (0.084 nm) compared to that of Ce^{4+} (0.098 nm), an almost linear decrease of lattice parameter (calculated from the main diffraction peaks) was expected to occur upon insertion of increasing amounts of ZrO_2 into the CeO_2 lattice [4].

On the other hand, Raman spectroscopy has proven to be a valuable tool in probing the determination of crystallite phase of ceria and zirconia polymorphs. Raman spectra in the 1700–150 cm^{-1} range were recorded for all the investigated samples. As for fresh CZ samples, Raman spectra (not shown) displayed typical bands corresponding to Ce/Zr solid solutions at 467, 635 and 297 cm^{-1} [20,21]. Pure ceria (CZ100/0) showed an intense band at 464 cm^{-1}, which corresponds to the symmetric O—Ce—O stretching mode. The band observed at 635 cm^{-1} corresponded to the non-degenerate Raman inactive LO (longitudinal optical) mode of ceria. This band arose due to the perturbation of M—O bond symmetry generated by oxygen vacancy. The appearance of the weak band at 297 cm^{-1} could be attributed to the displacement of oxygen atoms from their ideal fluorite type lattice of cerium oxide. No changes in this range were noticed for sulphated samples. However, additional Raman bands at 1020 and 1245 cm^{-1}, as shown in Fig. 2 for CZ50/50S sample, were observed. These bands were assigned to the presence of S-containing species, such as hydrated surface sulphates or hydrogen sulphate species [22–25]. These Raman results clearly suggested that the interaction of the oxides with sulphuric acid was essentially a surface process. The amount and nature of the sulphur species on the CZS catalysts was further examined by XPS. An enlarged image of the S2p photoemission spectra is given in Fig. 3. It was observed that the maximum binding energy peak was about 167.9–168.6 eV, which was assigned to sulphate species [26,27]. The deconvolution of this feature takes into account the known 2:1 intensity ratio between the S 2p1/2 and 2p3/2 spin–orbit states

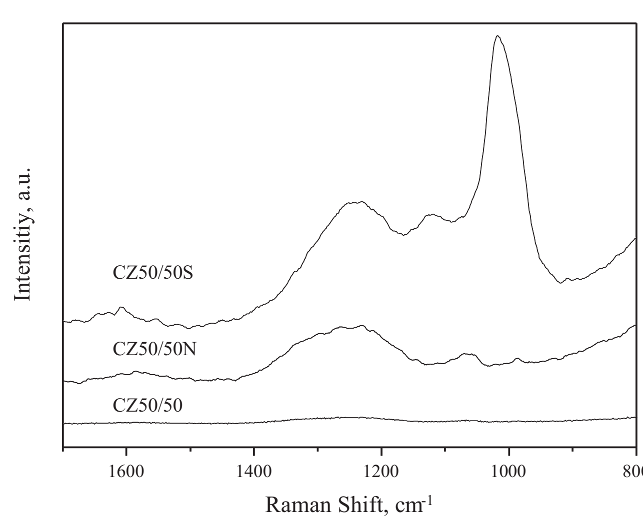

Fig. 2. Raman spectra for CZ50/50, CZ50/50S and CZ50/50N samples.

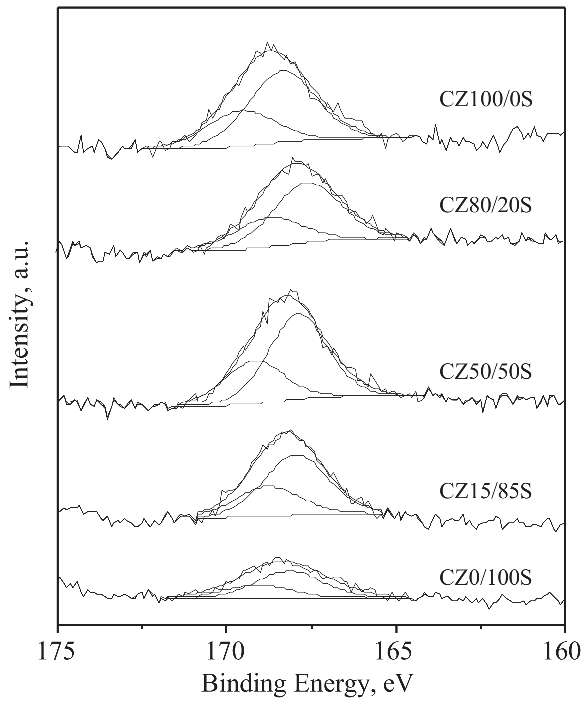

Fig. 3. S2p photoemission spectra of CZS samples.

and the known binding energy between these spin–orbit states of 1.18 eV. On the other hand, a slightly higher surface sulphur content was found (0.7–2 wt.%) in comparison with that determined by TGA–MS (0.6–1.3 wt.%). As aforementioned, this revealed that sulphate species mainly accumulated on the surface rather than entering into the lattice of the oxides.

The absence of structural changes after sulphur-doping was corroborated by XRD analysis (Fig. 4). No extra peaks ascribed to the presence of S-containing phases were observed in the range between (2θ) 5° and 80°, thereby suggesting that the sulphated species might exist as either surface species or amorphous bulk species. Moreover, the crystalline structure was maintained for all the samples. Consistently, the surface area of the Zr-rich mixed oxides (CZ50/50S, CZ15/85S and CZ0/100S) was not markedly affected with a decrease by about 5–10% after sulphation. This was in stark contrast with the observed loss of surface area shown by CZ100/0S, from 100 to 35 $m^2\,g^{-1}$, and by CZ80/20S from 100 to 80 $m^2\,g^{-1}$. The notable impact of sulphation on these two Ce-rich samples was in line with a moderate increase in their crystallite size, as calculated from the X-ray line broadening according to the Scherrer equation (Table 1). This phenomenon could be tentatively understood as chemical sintering induced by the strong acid. As for nitrated samples (CZN) similar conclusions could be drawn. Thus, no evident structural changes were detected for the mixed oxides after nitration. The vibrational frequency at 1275 cm^{-1} suggested the reduced presence of nitrate species [28–30] in agreement with TGA–MS results.

Temperature-programmed desorption of ammonia was used to evaluate the acidic properties of the mixed oxides in terms of overall acidity and acid strength distribution. Also some results on the nature of the acid sites present on the doped samples were provided by means of the adsorption of pyridine at 100 °C followed by Raman spectroscopy. The area under the TPD profile gave an estimation of the amount of acid sites in each sample (Fig. 5). In order to establish the strength of these sites the profiles were typically deconvoluted into three bands, which were correlated to weak, moderate and strong acidity with desorption peaks temperatures at 150, 250–300 and 350–450 °C, respectively.

As for fresh mixed oxides, it was found that total acidity markedly increased with zirconia content (Table 2). Thus, the highest acidity was observed for CZ15/85 followed by CZ50/50 [4].

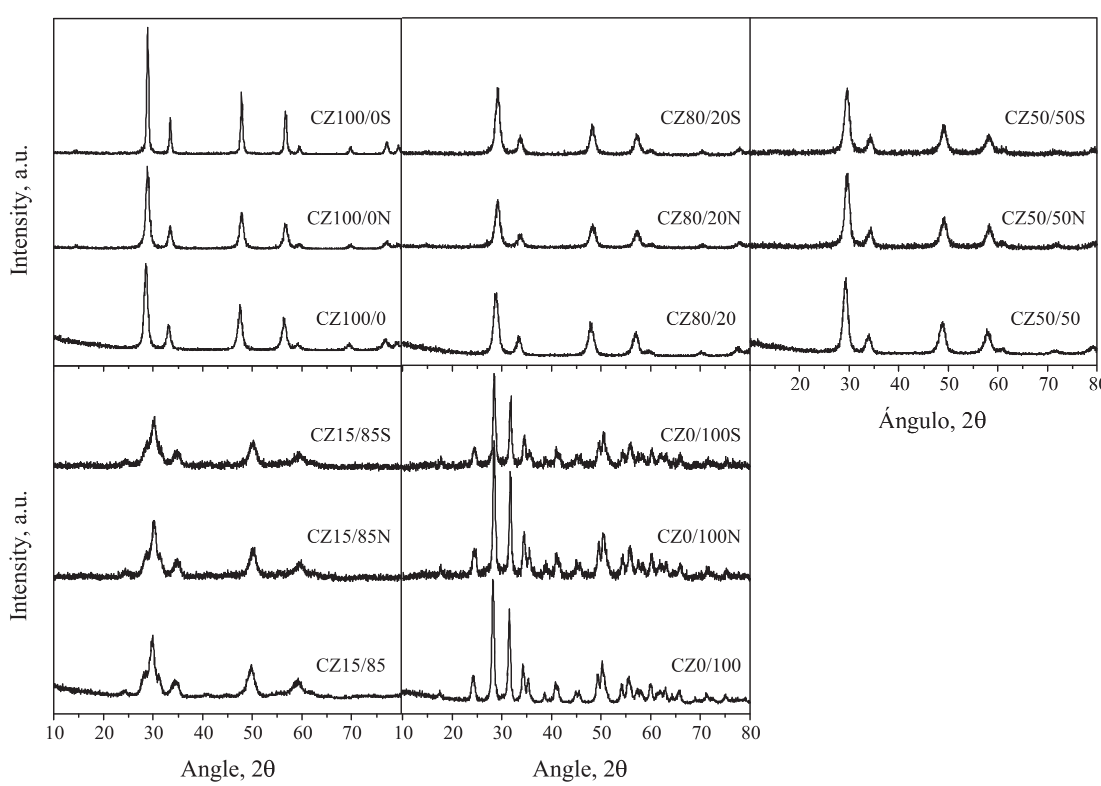

Fig. 4. XRD patterns for CZ, CZS and CZN samples.

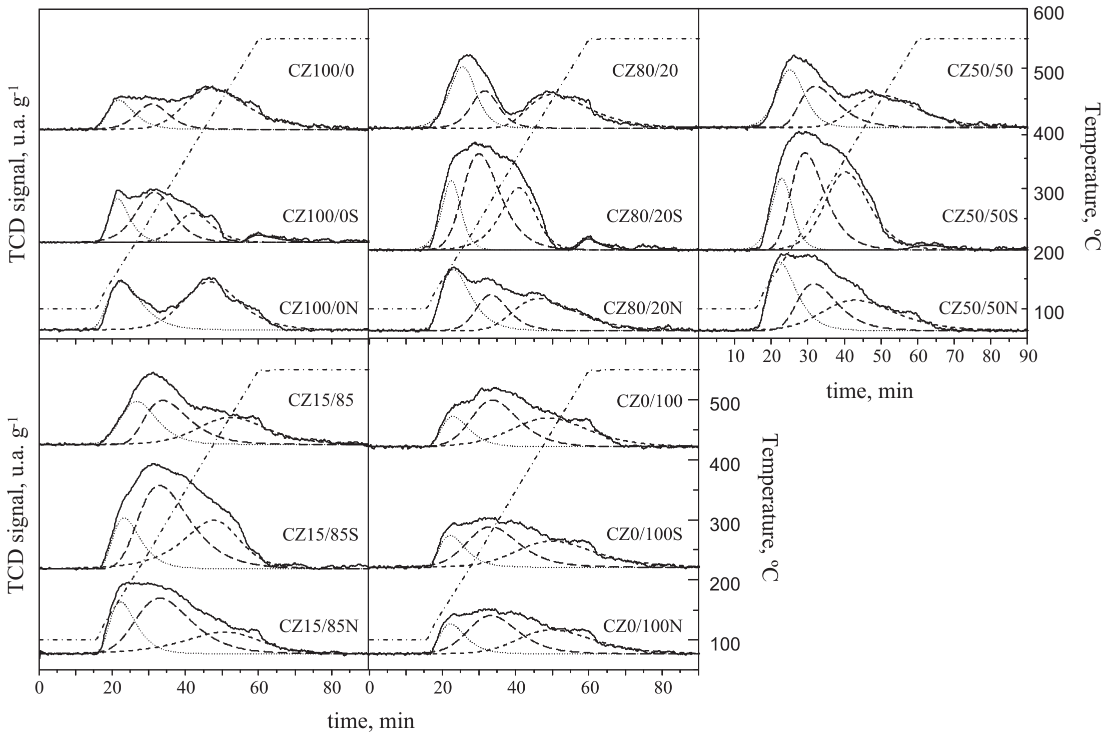

Fig. 5. NH_3-TPD profiles for CZ, CZS and CZN samples.

Moreover, the insertion of Zr into the ceria lattice led to an increase in the acid strength of the sites. After sulphation the acid properties of the oxides resulted notably affected whereas nitration appeared to provoke minimal changes, probably due to the low amount of N-species on the samples (Fig. 5). Thus, the overall acidity of the sulphated samples was increased. While this promoting effect was less pronounced on CZ100/0S (about 15%) and CZ0/100S (about 24%), a notable enhancement was found for the sulphated mixed oxides. The observed increase was relatively similar (about 100%) consistently with their similar sulphur content. Hence, the acidity of CZ50/50 and CZ15/85 varied from 233 and 249 μmol NH_3 g^{-1} to 461 and 506 μmol NH_3 g^{-1}, respectively. Another effect of sulphation was the higher concentration of acid sites able to retain adsorbed ammonia up to 250 °C (sites with a moderate/high acid strength). This marked effect of sulphation on the acidic characteristics of Ce-based catalysts was in fairly good agreement with the results recently found by Azambre et al. [25], Mejri et al. [31] and Gu et al. [32]. On the other hand, nitration also promoted the overall acidity of the starting oxides but to a significantly lower extent in comparison with sulphation. Also a significant increase in the amount of acid sites with moderate/high strength was noticed.

Apart from characterising the overall acidity and the acid strength of the doped samples, it could be also of special relevance to determine the nature (Brönsted or Lewis acidity) of these acid sites. In this sense, Raman spectroscopy using pyridine as a probe molecule was applied. When selecting the most appropriate Raman shift region for an unambiguous determination of the nature (type) of the acid sites, the attention was mainly focused on the 3000–3200 cm^{-1} range (which corresponded to the so-called ν_2 CH stretch mode) [33]. In this region, a considerably less marked overlap of the bands was found with respect to the 950–1050 cm^{-1} range (corresponding to ν_1 and ν_{12} ring-breathing modes), which could be also eventually used for discriminating between Brönsted and Lewis sites [34,35]. Thus, the band at about 3070–3085 cm^{-1} was assigned to pyridine adsorbed on Lewis sites while the peak at around 3090–3110 cm^{-1} was attributed to pyridine adsorbed on Brönsted sites [33].

Table 2
Acid properties for CZ, CZS and CZN samples.

Catalyst	Total acidity, μmol NH_3 g^{-1}	Weak acidity, μmol NH_3 g^{-1} (%)	Moderate acidity, μmol NH_3 g^{-1} (%)	Strong acidity, μmol NH_3 g^{-1} (%)
CZ100/0	187	34 (18.2)	38 (20.3)	115 (61.5)
CZ100/0S	215	48 (22.3)	102 (47.4)	65 (30.3)
CZ100/0N	237	87 (36.7)	–	150 (63.3)
CZ80/20	190	67 (35.3)	42 (22.1)	81 (42.6)
CZ80/20S	370	68 (18.4)	180 (48.6)	122 (33.0)
CZ80/20N	252	91 (36.1)	59 (23.4)	102 (40.5)
CZ50/50	233	73 (31.3)	69 (29.6)	91 (39.1)
CZ50/50S	461	82 (17.8)	226 (49.0)	153 (33.2)
CZ50/50N	328	104 (31.7)	102 (31.1)	122 (37.2)
CZ15/85	249	42 (16.9)	122 (49.0)	85 (34.1)
CZ15/85S	506	83 (16.4)	254 (50.2)	169 (33.4)
CZ15/85N	368	81 (22.0)	185 (50.3)	102 (27.7)
CZ0/100	205	32 (15.6)	86 (42.0)	87 (42.4)
CZ0/100S	279	46 (16.5)	118 (42.3)	115 (41.2)
CZ0/100N	254	43 (16.9)	109 (42.9)	102 (40.2)

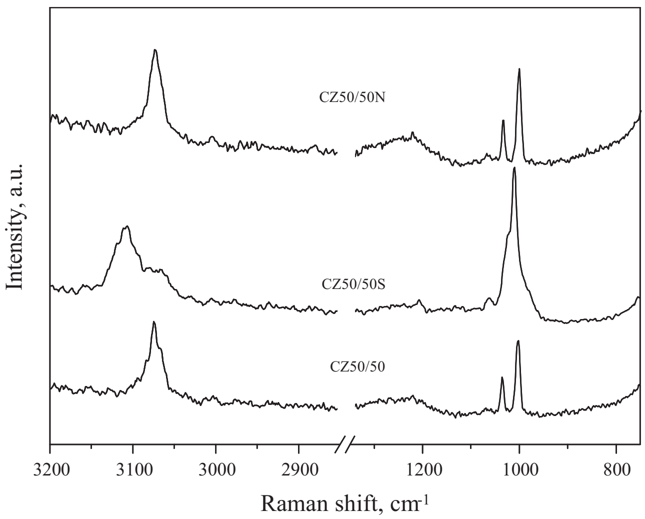

Fig. 6. Raman spectra of adsorbed pyridine on CZ50/50 samples.

Fig. 6 compares the Raman spectra of adsorbed pyridine on CZ50/50, CZ50/50S and CZ50/50N samples. Thus, it was observed that acid sites present on fresh CZ50/50 were almost exclusively Lewis-type in fairly good agreement with previous results obtained by infrared spectroscopy [36]. It must be pointed out that this spectrum was expectedly quite similar to that of CZ50/50N according to the less important influence of doping with HNO_3 as previously shown by bulk characterisation. However, substantial differences were noticed for the CZ50/50S sample. The formation of new Brönsted sites was clearly assessed as revealed by the intense band at 3110 cm^{-1}. These results were consistent with those previously reported for sulphated zirconia-based catalysts [25,37,38]. In fact, this sample contained both types of acid sites but with a larger contribution of Brönsted-type acidity. The change in the nature, from Lewis to Brönsted acidity, of the acid sites was also suggested by the modification of the spectra of CZ50/50S in the 950–1050 cm^{-1} range when compared with those of CZ50/50 and CZ50/50N samples.

The redox properties of the oxides were examined by temperature-programmed reduction (TPR) with hydrogen (5% H_2/Ar). Fig. 7 shows the TPR profiles of the fresh Ce/Zr catalysts. Firstly, it could be seen that the pure CeO_2 sample displayed a broad reduction profile with a low-temperature H_2 peak centred at around 480 °C, which was attributed to the reduction of the uppermost layers of Ce^{4+}, and a high-temperature H_2 peak centred at 870 °C approximately, which was associated with the bulk ceria reduction [39]. However, by incorporating zirconia into the ceria the H_2 consumption was greatly increased, and the temperature at which the bulk ceria reduction started was significantly lowered (550–560 °C). Hence, the profiles of the mixed oxides essentially showed a main broad reduction feature. The results demonstrated that the insertion of zirconium in the ceria lattice promoted the reduction of the cerium ions, firstly by making the surface reduction easier, and secondly by increasing the oxygen mobility in the bulk due to the lower charge/radius of Ce^{3+} with respect to that of Ce^{4+}, thereby accelerating the bulk reduction [40]. It was found that the reducibility varied with the composition, reaching a maximum for the CZ50/50 sample (1.14 mmol H_2 g^{-1}). Note that the reducibility of the pure ZrO_2 sample was expectedly rather low. Fig. 7 also includes the reduction profiles of CZN samples. A negligible alteration of the redox properties with respect to the fresh counterparts was noticed after nitration in line with the rather reduced presence of N-species.

Upon addition of sulphate species a larger H_2 consumption was noticed over the oxides (Fig. 7). This reduction process was observed to take place in the same temperature window as the reduction of the fresh samples. This indicated that, in addition to the reduction of cerium (Ce^{4+}) species, the simultaneous reduction of the sulphated species to give SO_2 and/or H_2S took place as well [41–43]. The occurrence of these two reduction processes involved a greater difficulty in interpreting the results from H_2-TPR analysis. It must pointed out that when evaluating the H_2 uptake the differences in thermal conductivity between H_2 (186 mW m^{-1} K^{-1}), SO_2 (8.6 mW m^{-1} K^{-1}), H_2S (14.6 mW m^{-1} K^{-1}) and Ar (17.9 mW m^{-1} K^{-1}) were assumed to be large enough to prevent a major interference of SO_2 and H_2S formation and H_2 consumption. In these experiments on-line mass spectrometry was also operated to identify gases formed in the TPR process. On the basis of the non-reducible character of pure zirconia, the TPR profile of CZ0/100S was useful for characterising the intrinsic reduction of the sulphated species. The reduction peak was about 600 °C and the specific H_2 consumption was about 0.03 mmol $g_{SO4}{}^{-1}$. SO_2 was the main reduction product although significant amounts of H_2S were detected as well. Note that this compound was also found during the thermal decomposition of the deposited sulphates as revealed by thermogravimetric analysis under inert conditions. Thus, its formation during the TPR experiment was probably a consequence of two simultaneous processes that involved both thermal decomposition and reduction of the grafted sulphate species.

The shape of the TPR profiles was relatively similar for all the sulphated Ce/Zr samples with a distinct peak at about 600–610 °C with a small shoulder at lower temperatures (555–575 °C). The profiles could be deconvoluted into two reduction bands which suggested that the overall reduction process consisted of two different reductions steps. The first one occurring at lower temperatures was ascribed to the reduction of Ce^{4+} to Ce^{3+} while the second one was associated with the reduction of surface sulphate species. The temperatures at which reduction occurred for sulphates on the various oxides were very similar [44]. Integration of the TPR profiles yields hydrogen consumption data compiled in Table 3. It was found that reduction consumed on the average five atoms H atoms per S atom of the surface sulphate (H/S = 5). This was an intermediate value between H/S = 4, which would involved a reduction process to SO_2 exclusively, and H/S = 8, which would correspond to a complete conversion of sulphate species to H_2S. Fig. 8 includes the MS profiles of the reduction of CZ50/50S sample. As aforementioned, conversion of sulphates to SO_2 (m/z = 48 and m/z = 64) was favoured although H_2S (m/z = 34) was also found in the product stream. Furthermore a good agreement in H_2 consumption was found between the values estimated for the fresh CZ50/50 and CZ15/85 samples and the values estimated from the low-temperature reduction peak for the sulphated CZS counterparts. This implied that the reduction of cerium was hardly affected by the presence of sulphate species. However, it was also true that the low-temperature reduction peak was shifted to slightly higher temperatures for CZ100/S and CZ80/20S catalysts. This effect was related to the growth of the crystallite size after sulphation (Table 1), which partially inhibited the reduction of cerium species.

3.2. Catalytic activity

The oxidation of 1,2-dichloroethane at constant weight hourly space velocity (635 g h $mol_{DCE}{}^{-1}$) and feed concentration (1000 ppm in air) was chosen as a measure to evaluate the impact of sulphation or nitration on the investigated Ce/Zr mixed oxides. Typically, catalytic activity was characterised by monitoring the rise in conversion as a function of temperature under given test conditions. A characteristic curve, referred to as the light-off or ignition curve (Fig. 9), was obtained. T_{50} and T_{90} (temperature at

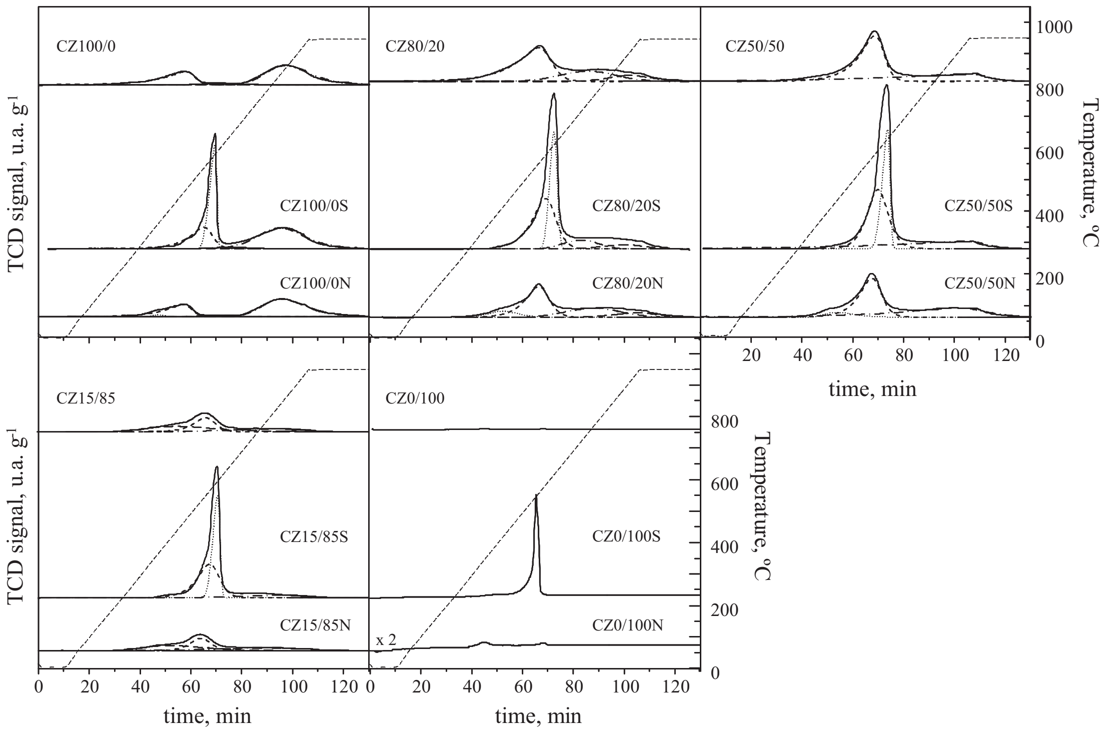

Fig. 7. H_2-TPR profiles for CZ, CZS and CZN samples.

which 50% or 90% conversion was reached) were used as indicatives of the relative reactivity of the examined catalysts. To provide a clearer picture of the influence of induced acidification on activity the corresponding T_{50} and T_{90} values were compared in Fig. 10. It should be pointed out that the possibility of homogeneous gas phase reactions at the reaction temperature range studied was checked through an experiment placing crushed quartz into the reactor tube. It was found that all the catalysed reactions needed significantly lower reaction temperatures than the homogenous reaction (>400 °C) irrespective of the catalyst examined.

The catalytic behaviour of the fresh samples is described in detail elsewhere [45]. Briefly, a noticeable catalytic performance was observed as revealed by the low temperatures required for the deep decomposition of the chlorinated compound (T_{50} values ranging from 300 to 360 °C compared with 450 °C for the homogeneous reaction). The CZ50/50 sample showed the highest activity. This notable catalytic behaviour highlighted the beneficial synergy that could be achieved by structural doping CeO_2 with ZrO_2. At temperatures below 400 °C, DCE conversion with the five oxide catalysts followed this trend: CZ50/50 > CZ15/85 > CZ50/20 > CZ100/0 > CZ0/100. Hence, the higher activity observed with respect to the pure oxides (CZ100/0 and CZ0/100) was associated with a suitable combination of surface acidity with relatively accessible lattice oxygen species. Accordingly, it was suggested that the first stage of the oxidation process was the adsorption of the chlorinated molecule on an acid site, which subsequently could be attacked by mobile oxygen species from the solid solution through a Mars-van Krevelen mechanism [36]. When examining the effect of sulphation or nitration on activity two different behaviours were noted. As shown by Figs. 9 and 10, nitration hardly affected the catalytic performance (occasionally even a slight decrease in activity was evident). In contrast, a substantial improvement was found for all the sulphated samples irrespective of its Ce/Zr ratio. This was consistent with the results reported by Wang et al. [46]. They found an increase in activity for H_2SO_4-treated $Cu/Mo/Al_2O_3$ catalysts in the oxidation of dimethyl disulphide. In contrast, no appreciable promotion was observed for samples treated with HNO_3.

Hence, T_{50} and T_{90} values were lowered by 55–90 °C and 70–120 °C, respectively. CZ50/50S exhibited the highest activity with a T_{50} value as low as 220 °C, followed by CZ15/85S and CZ80/20S. Total removal of DCE was achieved at 300 °C over CZ50/50S and CZ15/85S in comparison with 400 °C required over the corresponding fresh counterparts. Sulphated pure oxides

Table 3
Redox properties for CZ, CZS and CZN samples.

	CZ samples			CZS samples				CZN samples	
	H_2 uptake, mmol g_{cat}^{-1}	T, °C	H_2 uptake, mmol g_{cat}^{-1}	H_2 uptake, mmol g_{SO4}^{-1}	T^a, °C	T^b, °C	T^c, °C	H_2 uptake, mmol g_{cat}^{-1}	T^a, °C
CZ100/0	0.37	480	1.09	0.03	610		610	0.35	476
CZ80/20	0.99	557	1.91	0.03	605	575	605	0.95	550
CZ50/50	1.14	558	2.13	0.03	610	560	610	1.14	555
CZ15/85	0.54	550	1.44	0.03	600	555	600	0.53	540
CZ0/100	–	–	0.49	0.03	600	–	600	0.04	350

[a] Peak temperature of the overall reduction process.
[b] Peak temperature of the reduction of cerium species ($Ce^{4+} \rightarrow Ce^{3+}$).
[c] Peak temperature of the reduction of sulphate (or nitrate) species ($SO_4 \rightarrow SO_2+H_2S$).

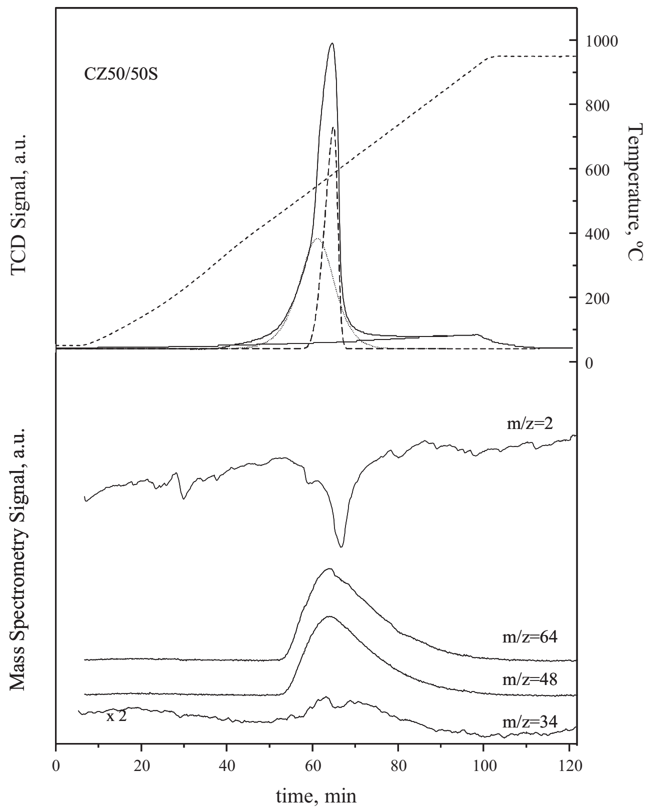

Fig. 8. H_2-TPR profile for CZ50/50S coupled to MS analysis.

exhibited a poorer performance. No change in conversion trend with respect to the fresh counterparts was noticed. Although out of the scope of this study it is worth pointing out that the activity of this sample was considerably higher than that displayed by other bulk oxide catalysts, such as dealuminated protonic zeolites, Mn/Zr mixed oxides, Mn_2O_3, κ-$CeZrO_4$ or Co_3O_4 [17].

Taking into consideration both characterisation and activity results the enhanced catalytic behaviour of sulphated CZ samples was mainly correlated with the promoted acidic properties of the oxides after sulphation. Not only the total amount of acid sites but also the average acid strength substantially increased. Moreover, a change in the nature of acid sites, from exclusively Lewis-type acidity on fresh samples to Brönsted/Lewis-type acidity on sulphated samples, was observed. In this sense, the importance of Brönsted acidity on zeolite catalysts for chlorinated VOC decomposition was already reported by López-Fonseca et al. [47]. On the other hand, since lattice oxygen mobility was previously observed to play a key role in chlorinated VOC oxidation over oxide catalysts, the fact that sulphation did not significantly interfere in the redox Ce^{4+}/Ce^{3+} couple was also a positive feature to lead to a highly active behaviour. In addition, it must be highlighted that after sulphation of CZ50/50 and CZ15/85 oxides no marked negative impact on textural and structural properties was found, which revealed a high stability of these specific compositions.

3.3. Product distribution and catalyst stability

High conversion is not the only criterion for determining good chlorinated VOC destruction catalysts. It is indeed useful to provide some basic information about the nature and the amount of reaction products, as the combustion of chlorinated VOCs may be accompanied by the concomitant production chlorinated by-products, sometimes more toxic and recalcitrant than the starting material. DCE oxidation over CZ50/50S gave rise to CO_2, CO, HCl and Cl_2 as major products. Nevertheless, the decomposition was accompanied by the generation of vinyl chloride at mild temperatures (85 ppm at 275 °C) as the main chlorinated compound. At 300 °C where DCE conversion was around 100% and vinyl chloride concentration was lower than 20 ppm, the favoured chlorine-containing deep oxidation product was HCl (92%) along with small quantities of Cl_2 (5%). This observation is quite important since the production

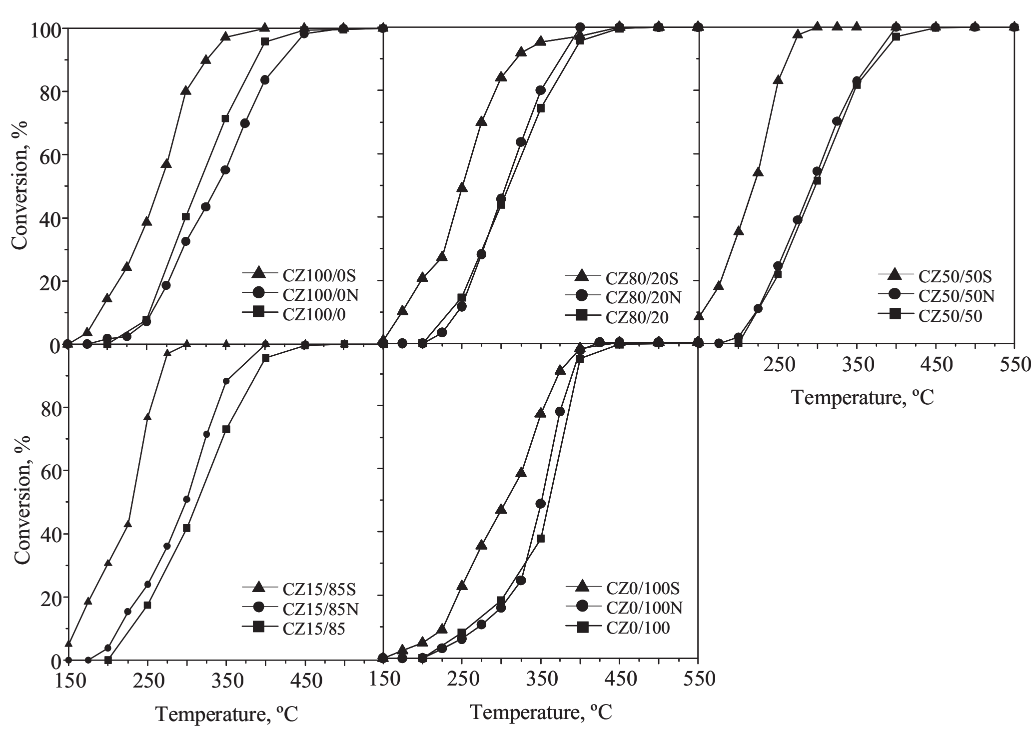

Fig. 9. Light-off curves of DCE oxidative decomposition over CZ50/50, CZ50/50S and CZ50/50N samples.

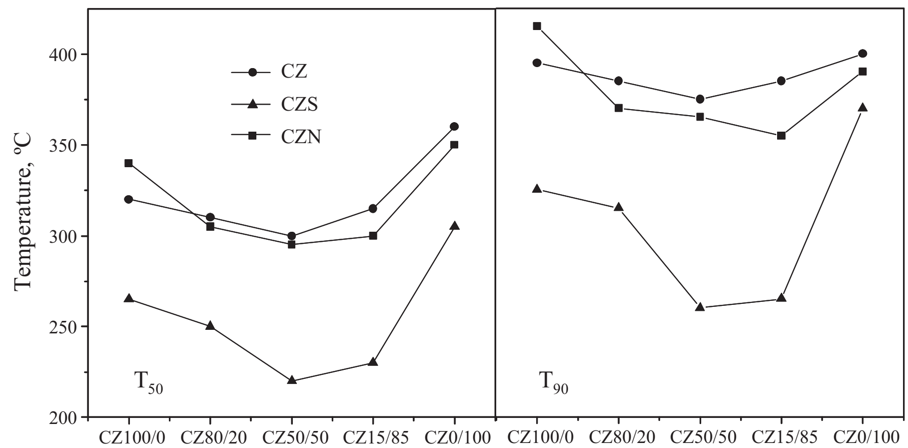

Fig. 10. Evolution of T_{50} and T_{90} values as a function of the oxide catalyst composition.

of chlorine is not desirable. Interestingly, the temperature required to DCE complete decomposition was low enough not to activate the oxidation of HCl to Cl_2 (Deacon reaction). Carbon atoms were converted into CO (69%) and CO_2 (27%). The nature of the decomposition products over CZ50/50 and CZ50/50N samples was similar to that observed over the CZ50/50S sample (CO, CO_2, HCl and Cl_2). Since the temperature needed for complete conversion was significantly higher (400 °C) the formation of C_{l2} was more noticeable with a selectivity close to 20%. Likewise, the selectivity to CO_2 increased up to 75%.

Finally, the stability of CZ50/50S was investigated by analysing the evolution of conversion with time on stream at 250 °C for 75 h (Fig. 11). This temperature was selected as it provoked a conversion of less than 100%, thus providing a more sensitive indication of changes of the catalyst performance with time on line. This experiment showed that conversion remained relatively stable with a slow decrease in activity from 55 to 47%. Probably the deposition of coke, about 2 wt.% as quantified by themogravimetry, was responsible for the observed decrease in activity. TGA–MS analysis revealed that these carbonaceous deposits could be completely burnt off at temperatures lower than 550 °C to yield CO_2 as deep oxidation product. This observation was important for the eventual regeneration step. Moreover, EDX analysis indicated the presence of a relatively reduced amount of Cl on the samples about 0.5 wt.%. XPS analysis suggested that the sulphate state was not apparently modified (the Sp3/2 peak position was about 168.6 eV). On the other hand, the same stability test (250 °C for 75 h) was carried out with the undoped catalyst (CZ50/50). Initially DCE conversion was about 25% and it gradually decreased to a stable lower value, close to 15%.

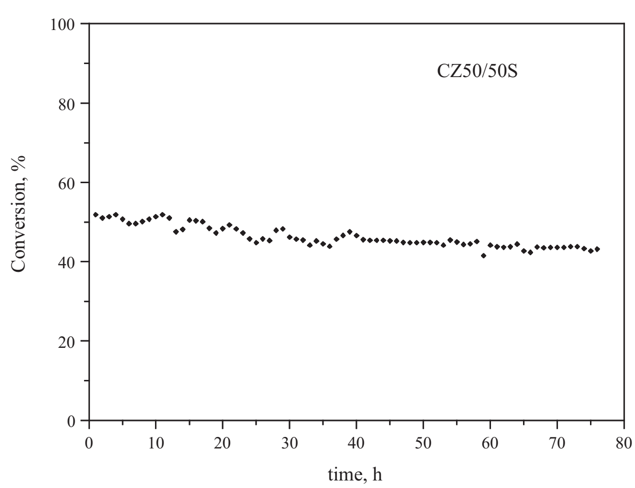

Fig. 11. DCE oxidative decomposition over CZ50/50S at 250 °C as a function of time on stream.

4. Conclusions

In this paper the effect of induced sulphation or nitration of ceria–zirconia mixed oxides (CeO_2, $Ce_{0.8}Zr_{0.2}O_2$, $Ce_{0.5}Zr_{0.5}O_2$, $Ce_{0.15}Zr_{0.85}O_2$ and ZrO_2) on the oxidative decomposition of 1,2-dichloroethane, selected as a model chlorinated VOC, was investigated. Sulphation via impregnation with H_2SO_4 resulted in a noticeable promotion of catalytic activity for all the investigated oxides. On the contrary, no appreciable effects on conversion were noticed after nitration. Doped $Ce_{0.5}Zr_{0.5}O_2$ and $Ce_{0.15}Zr_{0.85}O_2$ samples, with a sulphur content around 1.2–1.3 wt.%, decomposed the chlorinated feed at temperatures as low as 300 °C. As revealed by TGA–MS, Raman spectroscopy and XPS, thermally stable sulphates species were grafted after acid treatment followed by high-temperature (550 °C) calcination. Furthermore, no appreciable changes in both textural and structural properties were noticed except for sulphated CeO_2 and $Ce_{0.8}Zr_{0.2}O_2$. The higher catalytic activity was ascribed to the notable enhancement of the acidic properties of the mixed oxides. Hence, the total acidity was markedly increased. Also the concentration of acid sites with a moderate/high acid strength was superior. The generation of new Brönsted sites was observed as well. On the other hand, sulphation noticeably modified the reducibility of resultant oxides since grafted species were reduced to SO_2 and H_2S. Interestingly, sulphur-doping did not substantially alter the reduction step of Ce^{4+}/Ce^{3+} in comparison with the parent mixed oxides. In sum, it could be concluded that sulphation was an effective tool to improve the performance of Ce/Zr mixed oxides for chlorinated VOC abatement as a result of the promotion of the contribution of acid catalysis to the dual acid/redox decomposition mechanism. Another remarkable feature was the favoured selectivity to HCl at low temperatures. The most active sample, namely sulphated $Ce_{0.5}Zr_{0.5}O_2$, also showed a relatively stable performance.

Acknowledgements

The authors wish to thank the UPV/EHU and Gobierno Vasco (SAIOTEK S-PE11UN025) for the financial support. Technical and human support from SGIker (XRD (A. Larrañaga), Raman spectroscopy (A. Sarmiento) and XPS (M.B. Sánchez)) is also gratefully acknowledged.

References

[1] Thematic Strategy on Air Pollution, Communication from the Commission to the Council and the European Parliament, Commission of the European Communities, COM(2005) 446 final, Brussels, 2005.
[2] E.C. Moretti, Practical Solutions for Reducing Volatile Organic Compounds and Hazardous Air Pollutants, Centre for Waste Reduction Technologies of the American Institute of Chemical Engineers, New York, 2001.
[3] J.J. Spivey, in: G. Ertl (Ed.), Handbook of Heterogeneous Catalysis, vol. 5, Wiley-VCH Verlag, Weinheim, 2008, pp. 2394–2411.
[4] J.I. Gutiérrez-Ortiz, B. de Rivas, R. López-Fonseca, J.R. González-Velasco, Applied Catalysis A: General 269 (2004) 147–155.
[5] J.I. Gutiérrez-Ortiz, B. de Rivas, R. López-Fonseca, J.R. González-Velasco, Applied Catalysis B: Enviromental 65 (2006) 191–200.
[6] B. de Rivas, R. López-Fonseca, M.A. Gutiérrez-Ortiz, J.I. Gutiérrez-Ortiz, Applied Catalysis B: Enviromental 104 (2011) 373–381.
[7] B. de Rivas, R. López-Fonseca, C. Sampedro, J.I. Gutiérrez-Ortiz, Applied Catalysis B: Enviromental 90 (2009) 545–555.
[8] B. de Rivas, R. López-Fonseca, M.A. Gutiérrez-Ortiz, J.I. Gutiérrez-Ortiz, Applied Catalysis B: Enviromental 101 (2011) 317–325.
[9] B. de Rivas, C. Sampedro, R. López-Fonseca, M.A. Gutiérrez-Ortiz, J.I. Gutiérrez-Ortiz, Applied Catalysis A: General 417–418 (2012) 93–101.
[10] Q. Huang, X. Xue, R. Zhou, Journal of Molecular Catalysis A: Chemical 344 (2011) 74–82.
[11] W.B. Feaver, J.A. Rossin, Catalysis Today 54 (1999) 13–22.
[12] J.-N. Park, C.W. Lee, J.-S. Chang, S.-E. Park, C.-H. Shin, Bulletin of the Korean Chemical Society 25 (2004) 1355–1360.
[13] C. Gannoun, R. Deglaigle, P. Eloy, D.P. Debecker, A. Ghorbel, E.M. Gaigneaux, Catalysis Communications 15 (2011) 1–5.
[14] C. Gannoun, R. Deglaigle, P. Eloy, D.P. Debecker, A. Ghorbel, E.M. Gaigneaux, Applied Catalysis A: General (2012), http://dx.doi.org/10.1016/j.apcata.2012.08.034.
[15] K.S. Go, Y. Kim, S.R. Son, S.D. Kim, Chemical Engineering Science 65 (2010) 499–503.
[16] WHO Regional Office for Europe, Air Quality Guidelines, second ed., WHO Regional Publications, European Series, No. 91, Copenhagen, 2000 (Chapter 5.6).
[17] B. de Rivas, R. López-Fonseca, C. Jiménez-González, J.I. Gutiérrez-Ortiz, Journal of Catalysis 281 (2011) 88–97.
[18] R. Srinivasan, R.A. Keogh, D.R. Milburn, B.H. Davis, Journal of Catalysis 153 (1995) 123–130.
[19] H. Matsuhashi, H. Nakamura, T. Ishihara, S. Iwamoto, Y. Kamiya, J. Kobayashi, Y. Kubota, T. Yamada, T. Matsuda, K. Matsushita, K. Nakai, H. Nishiguchi, M. Ogura, N. Okazaki, S. Sato, K. Shimizu, T. Shishido, S. Yamazoe, T. Takeguchi, K. Tomishige, H. Yamashita, M. Niwa, N. Katada, Applied Catalysis A: General 360 (2009) 89–97.
[20] G. Colon, M. Pijolat, F. Valdivieso, H. Vidal, J. Kaspar, E. Finocchio, M. Daturi, C. Binet, J.C. Lavalley, R.T. Baker, S. Bernal, Journal of Chemical Society, Faraday Transactions 94 (1998) 3717–3726.
[21] B.M. Reddy, P.M. Sreekanth, P. Lakshmanan, A. Khan, Synthesis Journal of Molecular Catalysis A: Chemical 244 (2006) 1–7.
[22] M. Waqif, P. Bazin, O. Saur, J.C. Lavalley, G. Blanchard, O. Touret, Applied Catalysis B: Environmental 11 (1997) 193–205.
[23] J. Twu, C.J. Chuang, K.I. Chang, C.H. Yang, K.H. Chen, Applied Catalysis B: Environmental 12 (1997) 309–324.
[24] R. Flouty, E. Abi-Aad, S. Siffert, A. Aboukaïs, Journal of Thermal Analysis and Calorimetry 73 (2003) 727–734.
[25] B. Azambre, L. Zenboury, J.V. Weber, P. Burg, Applied Surface Science 256 (2010) 4570–4581.
[26] E.J. Romano, K.H. Schulz, Applied Surface Science 246 (2005) 262–270.
[27] A. Baylet, C. Capdeillayre, L. Retailleau, P. Vernoux, F. Figueras, A. Giroir-Fendler, Applied Catalysis B: Enviromental 96 (2010) 434–440.
[28] M.O. Symalla, A. Drochner, H. Vogel, S. Philipp, U. Göbel, W. Müller, Topics in Catalysis 42–43 (2007) 199–202.
[29] A. Urakawa, N. Maeda, A. Baiker, Angewandte Chemie 120 (2008) 9396–9399.
[30] E. Pretsch, P. Bühlmann, M. Badertscher, Structure Determination of Organic Compounds. Tables of Spectral Data, Springer-Verlag, Berlin, Heidelberg, 2009.
[31] I. Mejri, M.K. Younes, A. Ghorbel, P. Eloy, E.M. Gaigneaux, Journal of Porous Materials 17 (2010) 545–551.
[32] T. Gu, Y. Liu, X. Weng, H. Wang, Z. Wu, Catalysis Communications 12 (2010) 310–313.
[33] J. Lu, K.M. Kosuda, R. Van Duyne, P.C. Stair, Journal of Physical Chemistry C 113 (2009) 12412–12418.
[34] R. Ferwerda, J.H. van der Maas, F.B. van Duijneveldt, Journal of Molecular Catalysis A: Chemical 104 (1996) 319–328.
[35] P. Yuan, D.Q. Wu, H.P. He, Z.Y.Z.Y. Lin, Applied Surface Science 227 (2004) 30–39.
[36] B. de Rivas, R. López-Fonseca, J.R. González-Velasco, J.I. Gutiérrez-Ortiz, Journal of Molecular Catalysis A: Chemical 278 (2007) 181–188.
[37] M.I. Zaki, A.A.M. Ali, Colloids and Surfaces A 119 (1996) 39–50.
[38] J. Gao, Y. Qi, W. Yang, X. Guo, S. Li, X. Li, Materials Chemistry and Physics 82 (2003) 602–607.
[39] M. Boaro, M. Vicario, C. de Leitenburg, G. Dolcetti, A. Trovarelli, Catalysis Today 77 (2003) 407–417.
[40] S. Bernal, C. Blanco, J.J. Calvino, J.M. Gatica, J.A. Perez-Omil, J.M. Pintado, Topics in Catalysis. 28 (2004) 31–45.
[41] B.-Q. Xu, W.M.H. Sachtler, Journal of Catalysis 167 (1997) 224–233.
[42] H. Zhao, S. Bennici, J. Cai, J. Shen, A. Auroux, Journal of Catalysis 274 (2010) 259–272.
[43] P. Bazin, O. Saur, F.C. Meunier, M. Daturi, J.C. Lavalley, A.M. Le Govic, V. Harle, G. Blanchard, Applied Catalysis B: Environmental 90 (2009) 368–379.
[44] T. Luo, R.J. Gorte, Applied Catalysis B: Enviromental 53 (2004) 77–85.
[45] B. de Rivas, J.I. Gutiérrez-Ortiz, R. López-Fonseca, J.R. González-Velasco, Applied Catalysis A: General 314 (2006) 54–63.
[46] C.-H. Wang, C.-N. Lee, H.-S. Weng, Industrial Engineering Chemistry Research 37 (1998) 1774–1780.
[47] R. López-Fonseca, J.I. Gutiérrez-Ortiz, J.L. Ayastuy, M.A. Gutiérrez-Ortiz, J.R. González-Velasco, Applied Catalysis B: Enviromental 45 (2003) 13–21.